An investigation of halogen-bonding as a structure-directing interaction in dithiadiazolyl radicals.

*Mitchell A. Nascimento,[a] Elodie Heyer,[a] Robert J. Less,[b] Christopher M. Pask,[b,†] Ana Arauzo,[c] Javier Campo[c] and Jeremy M. Rawson.[a,b]**

a) Department of Chemistry and Biochemistry, The University of Windsor, 401 Sunset Avenue, Windsor, ON, CANADA N9B 3P4.

b) Department of Chemistry, Cambridge University, Lensfield Road, Cambridge, UK, CB3 0AG.

c) Instituto de Ciencia de Materiales de Aragón, CSIC-Universidad de Zaragoza, and Departamento de Física de la Materia Condensada, Facultad de Ciencias, University of Zaragoza E-50009 Zaragoza, Spain.

KEYWORDS: • dithiadiazolyl • halogen-bonding • polymorphism • supramolecular chemistry

ABSTRACT: The preparation and characterization of the halo-functionalized dithiadiazolyl radicals *p*-XC_6F_4CNSSN (X = Br (**1**) or I (**2**)) are described. Compound **1** is trimorphic. The previously reported phase **1α** ($Z' = 1$) comprises monomeric radicals whereas **1β** comprises a mixture of one cis-oid π*-π* dimer and one monomer ($Z' = 3$) and **1γ** exhibits a single cis-oid dimer ($Z' = 2$) in the asymmetric unit. We have only been able to isolate a single polymorph of **2**, isomorphous with **1α**. Both the bromo and iodo groups in **1** and **2** promote sigma-hole type interactions of the type C-X···N (X = Br, I), reflecting the increasing strength of this interaction for the heavier halo-derivatives. An analysis of the intermolecular forces using dispersion corrected DFT (UM06-2X-D3/LACV3P*) and compared to a unified pair potential model (UNI) embodied in the crystallographic software Mercury. While there is a correlation between DFT and UNI force-field models, there are some discrepancies, although both reveal that a number of intermolecular contacts beyond the sum of the van der Waals radii are significant (> 5 kJ mol^{-1}). An NBO analysis of the intermolecular interactions reveal lone pair donation from the heterocyclic N atom to C-X or S-S σ* orbitals contributes to these intermolecular interactions with relative energies in the order C-I > S-N-II > C-Br > SN-III. The magnetism of **2** reveals a broad maximum in χ around 20 K indicative of short-range antiferromagnetic interactions. These are supported by DFT calculations which reveal a set of three significant exchange interactions which propagate in two dimensions.

INTRODUCTION

In the last few decades there has been enormous progress in the emerging field of molecule-based materials. For crystalline solids the identification and application of new *supramolecular synthons* is central to our understanding of the non-covalent forces between molecules which dictate structure and function.[1] While hydrogen bonding is ubiquitous in this area,[2,3] considerable efforts have been made to identify other important structure-directing interactions.[4] The weak nature of intermolecular non-covalent interactions can lead to many near equi-energetic packing arrangements, reflected in polymorphism.[5] For radicals the subtle changes in molecular structure can lead to dramatic changes in materials properties. For example, when radicals adopt π-stacked structures efficient orbital overlap leads to increased band width and a small energy barrier for charge transport,[6] whereas a narrow band of localized spins occurs when overlap is reduced.[7] The identification of strong supramolecular synthons provides a library of functional groups which can be used to impart some degree of structural control over the solid state packing. In the current paper we examine the use of halogen-bonding[8] as a potential structure-directing group for a family of thermally robust radicals, the dithiadiazolyls (DTDAs).[9] The latter radicals have been implemented as building blocks in the design of molecular conductors[6] and magnets,[7,10] as ligands in both coordination chemistry[11,12] and organometallics.[13] More recently several studies have identified examples of enantiotropic polymorphs[14] of DTDA radicals where reversible solid-to-solid phase transitions can occur between polymorphs which have been associated with both displacive (translational)[15-17] and rotational motion.[18] Approaches to control the solid state structures of DTDA radicals have examined modes of self-recognition between DTDA radicals as well as the presence of other structure-directing groups.[19,20] Of these structure-directing groups the most well-established is the CN···S interaction which has been implemented to generate

supramolecular chains.[21-28] In the majority of cases DTDA radicals adopt π*-π* dimer motifs in which the pancake bonding[29,30] gives rise to a singlet ground state configuration, quenching the radical paramagnetism. The strong tendency of these radicals to dimerize, predominantly in a cis-oid cofacial fashion can itself be considered as a strong supramolecular synthon (ΔH_{dim} in solution around 35 kJ·mol^{-1}).[31-33]

In the context of the current studies, the effect of halogenated aryl substituents on bonding has been explored. A series of studies of fluoroaryl radicals have been isolated and their structures are largely dictated by self-recognition modes between DTDA radicals (Fig. 1). Notably the 2′,6′-$F_2C_6H_3CNSSN$ was found to be trimorphic and it is particularly noteworthy that the γ-phase has two molecules in the asymmetric unit ($Z' = 2$), comprising one monomeric radical and half a trans-antarafacial dimer, reflecting the fine energetic balance between π*-π* dimerization and other packing factors. Similar behaviour was also observed in *p*-$EtOC_6F_4CNSSN$ which comprised three phases with the α-phase exhibiting pure dimers ($Z' = 2$) while the β-phase ($Z' = 6$) comprises two dimers and two monomers and undergoes a reversible phase transition to the γ-phase ($Z' = 14$) upon cooling, which comprises six dimers and two monomers. Indeed the propensity for DTDA radicals to exhibit structures with large Z' values has been noted.[34] For several perfluoroaryl derivatives, *p*-XC_6F_4CNSSN (X = CN, NO_2, Br and NCC_6F_4) dimerization has been fully suppressed and in some cases this has led to long range magnetic order, whereas in others low dimensional magnetic behaviour is observed.[28,35,36] For dichloroaryl derivatives,[37] $Cl_2C_6H_3CNSSN$, the chloroaryl groups take on a more structure-directing role in which there is a tendency to exhibit (i) S···Cl contacts close to the DTDA molecular plane and (ii) π-stacked structures driven by the propensity for chloro-aryl derivatives to adopt the so-called β-sheet motif.[38,39] In recent years, the structure-directing halogen bonding interaction has been identified[8]

and we were interested to explore how such halogen bonding motifs might be manifested in directing the structures of DTDA radicals.

EXPERIMENTAL

The starting materials Ph_3Sb and $Li[N(SiMe_3)_2]$ (Sigma) and C_6F_5CN (Oakwood) were used as received. The nitriles, *p*-XC_6F_4CN (X = Br, I) were prepared according to the literature method.[40] All solids were handled under a nitrogen atmosphere using a MBraun Labmaster glovebox while solvents were dried and degassed using an Innovative Technology solvent purification system. Temperatures below ambient were achieved using a Fisher Scientific Isotemp 4100 R28 recirculating chiller using isopropanol. Elemental analyses were measured by combustion using a Perkin Elmer 2400 Series II CHNS/O Analyzer, operated in CHN mode. Samples of *ca*. 1.8 - 2.0 mg, were sealed in aluminium capsules and weighed using a Perkin Elmer AD-6 Autobalance located in a glove-bag under a nitrogen atmosphere. EPR spectra were obtained on a Bruker EMXplus X-band EPR spectrometer running at ca. 9.8 GHz, utilizing a high sensitivity cylindrical cavity fitted with a liquid nitrogen cryostat with a Eurotherm temperature control unit, along with a high precision microwave frequency counter. Solution samples for EPR were prepared in quartz tubes (Wilmad).

Preparation of (p-$BrC_6F_4CNSSN)_2$ (1): *p*-BrC_6F_4CN (0.500g, 1.97 mmol) was added to a solution of $Li[N(SiMe_3)_2]$ (0.330 g, 1.97 mmol) in Et_2O (20 mL). The reaction mixture turned orange and was stirred for 4h at room temperature, cooled to 0 ^oC and SCl_2 (0.26 mL, 0.426 g, 4.14 mmol, 2.1 eq.) added slowly. The solution was allowed to warm to room temperature and stirred for 18h. The resultant orange precipitate, [*p*-BrC_6F_4CNSSN]Cl, was filtered, washed with Et_2O (2 × 20 mL) and dried *in vacuo*. A sample of [*p*-BrC_6F_4CNSSN]Cl (0.500 g, 1.36 mmol) and Ph_3Sb (0.240 g, 0.68 mmol) were combined in a Schlenk tube under a nitrogen atmosphere and

manually mixed to ensure homogeneous distribution of reducing agent throughout the chloride salt. The Schlenk tube was then heated to 70 °C with stirring to generate a deep homogenous purple oil. The radical was sublimed under static vacuum at 50 °C onto a cold-finger maintained at −2 °C. The cold-finger was removed intermittently and the sublimate removed affording a mixture of **1α** and **1β** as lustrous red needles and red blocks, respectively. Total yield = 251 mg (62% based on [*p*-BrC_6F_4CNSSN]Cl). When the sublimation temperature was raised to 75 °C and the cold-finger temperature was maintained at -2 °C, **1γ** was obtained as dark red blocks. Elemental analysis calc. for $C_7BrF_4N_2S_2$: C 25.32%, H 0.00%, N 8.44%; found: C 25.30 %, H 0.00%, N 8.43%; EPR (X-band, CH_2Cl_2, 298 K); g = 2.0097, a_N = 4.9 G; MS(EI+) *m/z* = 330.8622 (M^+), 284.9 (M^+ − SN), 252.9 (M^+ − SSN), 226.9 (M^+ − CNSSN) [All peaks quoted for the ^{79}Br isotopomer]; IR (ν_{max}, cm^{-1}, nujol): 1639(s), 1502 (s), 1416(s), 1361(s), 1246(s), 1170(m), 1059(m,sh), 977(s), 854(m), 819(s), 796(s), 751(s, sh), 724 (s, sh), 643 (m, sh).

Preparation of (p-$IC_6F_4CNSSN)_2$ (2): The radical *p*-IC_6F_4CNSSN (**2**) was prepared in an analogous fashion to **1**. The radical was sublimed at 70 - 75 °C with the cold finger maintained between −2 and +12 °C. The cold-finger was removed intermittently and the sublimate removed. Total yield = 277 mg (31 %) based on [*p*-IC_6F_4CNSSN]Cl (1.30 g, 0.0031 mol). Elemental analysis calc. for $C_7IF_4N_2S_2$: C 22.18%, H 0.00%, N 7.39%; found: C 21.76 %, H 0.27%, N 7.09%; EPR (X-band, CH_2Cl_2, 298 K): g = 2.0099, a_N = 5.2 G; MS(EI+) 379 (M^+), 333 (M^+ − SN), 301 (M^+ − SSN).

Crystallographic studies: Crystals of **1β**, **1γ** and **2** were mounted on a cryoloop and measured on a Bruker D8 Venture equipped with a cryostream low temperature device (Oxford Instruments). Data were measured using APEX3,[41] integrated using SAINT,[42] an absorption correction applied using SADABS[43] and the structures determined using intrinsic phasing (SHELXT).[44] The

structures were refined using SHELXL 2017.[45] A summary of the crystallographic studies are presented in Table 1 along with previously reported data for **1α**. The structures have been deposited at the CCDC (deposition numbers: 1970967-1970969).

RESULTS

The starting nitriles, *p*-XC_6F_4CN were prepared according to the literature method by nucleophilic aromatic substitution on C_6F_5CN with one equivalent of X^- (X = Br, I) which occurs preferentially *para* to the nitrile.[40] Nitriles were purified by sublimation prior to use. Treatment of the resultant nitrile with $Li[N(SiMe_3)_2]$ followed by condensation with a slight molar excess of SCl_2 (2.1 – 2.2 equivalents) led to the 1,2,3,5-dithiadiazolylium chloride salts.[46] We explored several approaches to reduction using a range of reducing agents (Ag, $Na_2S_2O_4$, Zn/Cu couple, Ph_3Sb) and solvents (SO_2, THF, MeCN). EPR studies clearly revealed radical generation in all cases but recovered yields after sublimation were typically poor (< 10%). Haynes' "solvent-free" reduction method using molten Ph_3Sb as both reductant and solvent provided a more efficient approach.[47] Using this approach, radicals **1** and **2** were isolated as crystalline solids in 31 – 62% recovered yield. They were characterized by their diagnostic EPR spectra (g ~ 2.01, a_N ~ 5 G), a molecular ion and fragmentation pattern in the mass spectrum with appropriate isotopomer ratios, elemental analysis as well as structure determination by X-ray diffraction.

A number of studies have identified the propensity for polymorphism in DTDA radicals.[15-18,21-28,36,48-50] Crystallization of DTDA radicals by sublimation is dependent upon the equilibrium between the gas phase and the solid state. Gibb's phase rule[5] relates the number of phases present (P) to the number of components (C) and the number of degrees of freedom (F):

$$P + F = C + 2 \qquad \text{Eqn. 1.}$$

For radical sublimation we have a single component system (C = 1) and Eqn 1 simplifies to:

Table 1: Crystal data for compounds **1** – **3**.

Compound	1α	1β	1γ	2
Formula	$BrC_7F_4N_2S_2$	$BrC_7F_4N_2S_2$	$BrC_7F_4N_2S_2$	$IC_7F_4N_2S_2$
Crystal system	Orthorhombic	Monoclinic	Orthorhombic	Orthorhombic
Space Group	*Aba*2	$P2_1/n$	*Pbca*	*Aba*2
T (K)	150(2)	170(2)	170(2)	170(2)
a/Å	8.263(2)	7.2487(3)	17.6032(10)	8.5315(5)
b/Å	20.426(4)	16.2492(5)	11.1439(5)	20.4878(11)
c/Å	11.556(2)	24.7655(9)	19.8350(10)	11.6808(6)
α/°	90	90	90	90
β/°	90	90.799(2)	90	90
γ/°	90	90	90	90
V/Å^3	1950.4(7)	2916.74(18)	3891.0(3)	2041.66(19)
Z (Z′)	8 (1)	12 (3)	16 (2)	8 (1)
D_C	2.262	2.269	2.268	2.467
μ/mm^{-1}	4.672	4.681	4.684	3.573
F(000)	1272	1908	2544	1416
Crystal size	0.35 × 0.25 × 0.20	0.28 × 0.12 × 0.05	0.19 × 0.16 × 0.07	0.23 × 0.20 × 0.02
$\theta_{min} - \theta_{max}$	3.17 – 27.51	2.768 – 26.452	2.949 – 24.754	3.107 – 27.482
Index ranges	$0 \le h \le 10$ $-26 \le k \le 0$ $-14 \le l \le 14$	$-9 \le h \le 9$ $-20 \le k \le 20$ $-30 \le l \le 30$	$-20 \le h \le 20$ $-11 \le k \le 13$ $-23 \le l \le 23$	$-11 \le h \le 11$ $-26 \le k \le 26$ $-12 \le l \le 15$
Reflections collected	2292	53186	40219	13437
Independent reflections	2175	5981	3325	2169
R_{int}	0.0449	0.0661	0.0925	0.0558
Data/restraints/parameter	2175/1/145	5981/0/433	3325/0/289	2169/1/146
Goodness of fit, *S* (all)	1.026	1.005	1.057	1.045
R_1 ($I > 2\sigma(I)$)	0.0643	0.0265	0.0299	0.0278
wR_2 (all)	0.1428	0.0558	0.0566	0.0696
Flack parameter	-0.02(2)	n/a	n/a	-0.02(4)
Max/min residual electron density	+0.91, -0.59	+0.33, -0.39	+0.36, -0.54	+0.58, -0.85
Reference	Ref. 35	This work	This work	This work
CSD Deposition #		1970968	1970967	1970969

$$P = 3 - F \qquad \text{Eqn. 2}$$

Since the number of degrees of freedom (intrinsic variables – temperature, pressure, concentration) cannot be negative there cannot be more than three phases present at any one time. In the case of sublimation at constant temperature and pressure, we can have a maximum of two solid phases (polymorphs) in equilibrium with the gas phase. These are known as concomitant polymorphs.[51,52] This does not preclude more than two polymorphs existing, but the other polymorphs must be formed under a separate set of conditions of temperature and/or pressure. For sublimation *in vacuo*,

a search for new polymorphs is most likely successful by screening across the temperature regime. This normally leads to another layer of complexity: During sublimation the substrate is normally heated at temperature T_2 to vaporize it into the gas phase and an equilibrium can be envisaged between solid and vapor at T_2. Condensation and crystal growth typically occur onto a cold finger or other substrate at a lower temperature, T_1. While each may be considered an equilibrium process with equilibrium constants K_1 and K_2, these two processes are not independent with material passing from the vaporization region (T_2) to the crystallization region (T_1). Provided T_2 and T_1 are similar then it is likely that the system is under thermodynamic control (all systems in equilibrium). Conversely, for larger temperature gradients, the rate of vaporization might be faster than the rate of crystallization and we may move into a kinetically rather than thermodynamically controlled regime. Within the context of these current studies we have been particularly interested to exploit these ideas to identify new paramagnetic DTDA radicals. Previous work has shown that multi-center pancake bonding, which quenches the radical paramagnetism in DTDA radicals, is enthalpically favored ($\Delta H_{dim} \sim 35$ kJ mol^{-1} in solution). Entropically-favored phases which contain one or more un-dimerized radicals are therefore likely at elevated temperatures. Among the possible modes of association (Fig. 1), a search of the CSD reveals a strong preference for the cis-oid dimerization mode and the propensity to form the *cis* π*-π* dimer motif can be considered a supramolecular synthon in its own right. Approaches to destabilize π*–π* dimers have been sought to assist the successful identification of new paramagnetic phases. In this context substitution in the 2′,6′-positions of an aryl substituent have led to steric and/or electronic repulsion between the *ortho*-fluoro substituents and the heterocyclic N atoms of the DTDA ring. We have had some success in isolating a series of *p*-XC_6F_4CNSSN radicals (X = CN, NO_2, Br and NCC_6F_4)[36-39,53] in which there is a large torsion angle between perfluoroaryl and DTDA rings leading to monomeric

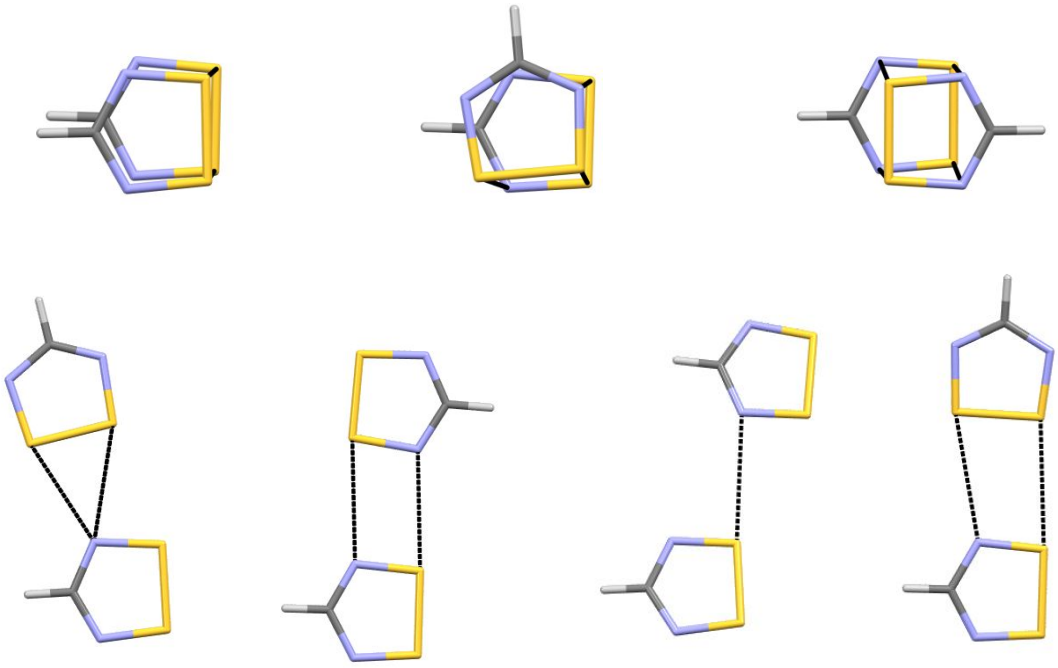

Figure 1: (top) from left to right common cis-, twisted- and trans-cofacial π*-π* dimers; (bottom) from left to right common non-covalent supramolecular modes of association (SN-I to SN-IV respectively).

DTDA radicals which retain their paramagnetism in the solid state. In several cases suppression of dimerization appears associated with the opportunity to form an alternative set of structure-directing contacts, such as CN···S,[21-28] which are comparable with or superior to the π*-π* dimerization process. One set of intermolecular interactions which has attracted recent interest is the halogen bond[8] in which there is polarization of the electron density around the halogen, typically manifested in a depletion of charge opposite the C-X bond and a build-up of electron density perpendicular to it. This leads to a directional C-X···D interaction to an electron-rich donor (D) in which some degree of charge-transfer of the lp(D)→σ*(C-X) type contributes to this interaction. Generally speaking the softer more polarizable halogens form stronger C-X···D interactions and we were intrigued to probe the structures of the derivatives *p*-XC_6F_4CNSSN (X

= Br, I), particularly since *p*-BrC_6F_4CNSSN was previously identified to not only be monomeric[36] but also exhibits a C-Br···N halogen bond contacts to the DTDA N atom.

Polymorphs of p-BrC_6F_4CNSSN (1): The α-phase of *p*-BrC_6F_4CNSSN (**1α**) was reported in 1999 and was prepared by high temperature gradient sublimation along a glass tube (120 °C, 10^{-1} torr).[35] The current studies probed other sublimation conditions: Vacuum sublimation of *p*-BrC_6F_4CNSSN using a bath temperature of +50 °C and cold finger temperature of −2 °C yielded a mixture of **1β** alongside the known polymorph **1α** (the major product based on PXRD studies, SUP-4). Further attempts to adjust the sublimation conditions to obtain pure **1β** were undertaken, but when the bath temperature was raised to 75 °C and cold finger temperature was maintained at −2 °C and left for 18 hours, crystals of **1γ** were isolated which could not be readily distinguished visually from crystals of **1β** except for being slightly darker in color. Variable temperature PXRD studies on **1** (predominantly **1α**) (25 to 75 °C) showed no evidence for a phase transformation across this temperature range (SUP-4).

The α-phase of *p*-BrC_6F_4CNSSN (**1α**) has been reported previously and is included here merely for comparison with the structures of **1β**, **1γ** and **2**. The structure of **1α** adopts the orthorhombic space group *Aba*2 with one molecule in the asymmetric unit. Unlike most DTDA radicals there is no π*–π* dimerization evident for this phase. The twist angle between aryl and DTDA ring planes is large (51.77°). The heterocyclic ring N atoms are involved in two sets of sigma-hole type interactions. The first of these is an established N···Br-C halogen bond[8] in which the C-Br···N angle and Br···N contact distance (162.8(4)°, 3.139(9) Å) are directly comparable with other C-Br···N contacts reported in the literature (mean 160.8° and 3.19 Å, see SUP-1). The second

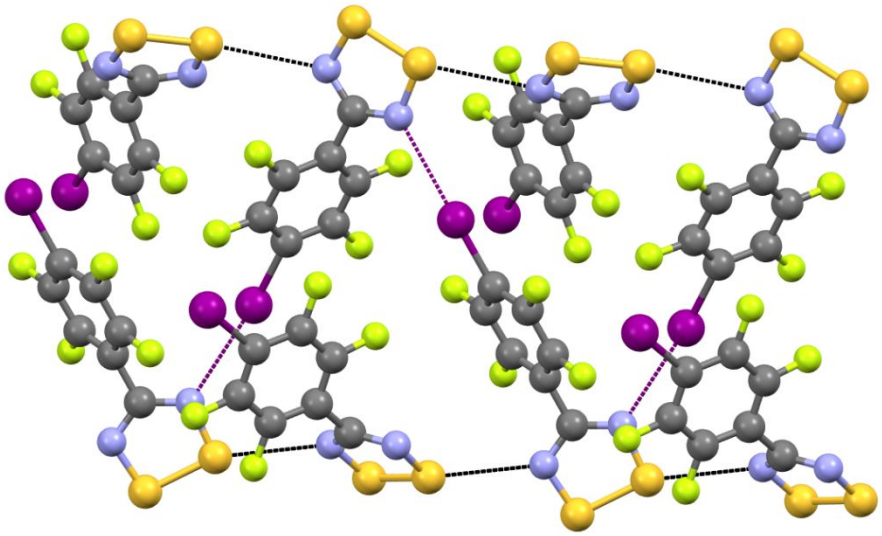

Figure 2: Packing of **2** highlighting N···I contacts (purple) and N···S contacts (black). The isomorphous bromo derivative **1α** adopts the same packing motif.

involves an S-S···N interaction (S···N at 3.17(1) Å, S-S···N at 160.2°) Such interactions have been recognized as structure-directing synthons in DTDA chemistry (SN-III, Fig. 1).[21-28] This can be considered as comparable to a halogen bond, involving charge transfer from the N lone pair to the S-S σ* orbital (*vide infra*). The structure of **1α** is isomorphous with the iodo derivative **2** (Fig 2). A search of the CSD for interactions between N atoms and a disulfide bond identifies two distinct categories of such S-S···N interactions which are clearly defined by their angular dependence (SUP-2), comprising a grouping around a mean of 162° (mean deviation ± 9°, such as SN-II and SN-III, Fig. 1) and a second group around a mean of 85° (mean deviation ± 13°, such as SN-IV, Fig. 1).

The β-phase of *p*-BrC_6F_4CNSSN crystallises in the monoclinic $P2_1/n$ space group with three molecules in the asymmetric unit ($Z' = 3$) (Fig. 3). These comprise a cis-oid (*p*-$BrC_6F_4CNSSN)_2$ dimer and a monomeric *p*-BrC_6F_4CNSSN radical as the structural building blocks. Within the dimer the angles formed between the DTDA and perfluoroaryl rings are 35.34 and 25.66°

respectively, while the angle between DTDA and perfluoroaryl planes in the monomer is 39.0°. The intra-dimer S···S contacts are unexceptional for such cis-oid multi-centre bonding interactions at 3.060(1) and 3.098(1) Å. Cis-oid dimers are linked through a combination of C-Br···N halogen bonds and SN-II-type[19] (Fig. 1) S···N interactions. Both these C-Br···N and S···N contacts are less than the sum of the van der Waals radii [Br3···N31 and Br2···N21 at 3.376(2) and 3.228(2) Å and C24—Br2···N21 = 163.5° and C34—Br3···N31 = 156.8°; S22···N32 at 3.353(2) Å and N22···S32 at 3.216(2) Å with S-S···N angles of 165.32(5) and 170.59(5)° respectively]. These two sets of interactions propagate through the lattice to generate a honeycomb-like motif (Fig. 3). The third crystallographically independent molecule of **1** is linked to these dimers through an SN-I type interaction [3.084(2) and 3.212(2) Å for N11···S21 and N11···S22 respectively] and a corresponding pair of S···S contacts [3.566(1) and 3.3321(9) Å for S11···S31 and S11···S32 respectively] (Fig. 4a). Pairs of monomeric radicals are located about an inversion centre which are supported through dipole-dipole interactions with closest contacts (black) being C14···S12 at 3.470(3) Å and C15···N12 at 3.243(4) Å (Fig. 4b).

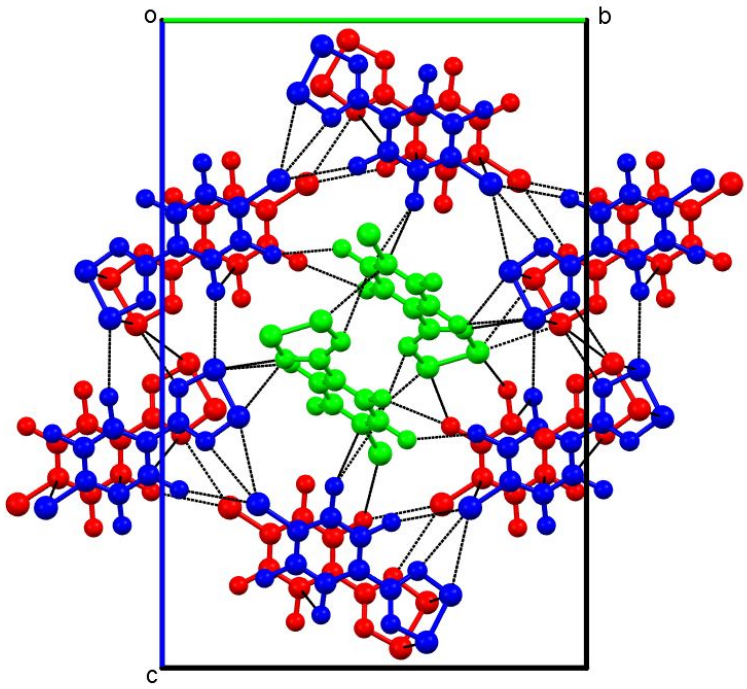

Figure 3: Crystal structure of **1β** with crystallographically independent molecules color-coded. The three molecules in the asymmetric unit comprise a π-dimer (red and blue) and a monomer (green). Dotted lines correspond to intermolecular contacts less than the sum of the van der waals radii.

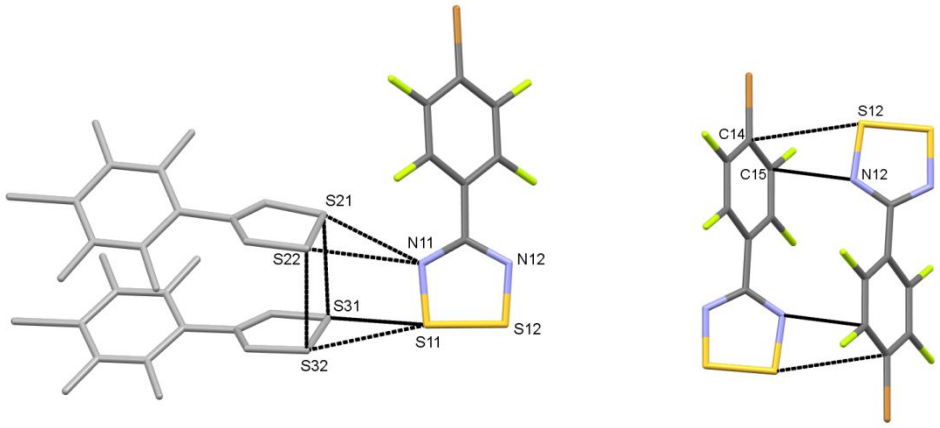

Figure 4: Intermolecular interactions in **1β**: (left) interaction between the monomeric molecule of **1** (colored) and the π*–π* dimers (gray); (right) centrosymmetric interaction between monomers.

The γ-phase of *p*-BrC_6F_4CNSSN (**1γ**) crystallises in the orthorhombic space group *Pbca* with two molecules in the asymmetric unit ($Z' = 2$). These two molecules form a cis-oid dimer similar to that found in **1β** with S···S contacts of 2.993(1) and 3.133(1) Å. The twist angles between DTDA and the perfluoroaryl rings are 35.78 and 41.09° for molecules containing S11 and S21 respectively. These dimers associate through a centrosymmetric pair of S-S···N contacts at 3.135(3) and 3.240(3) Å (corresponding angles are 162.78(6) and 171.52(7)°) to form a tetrameric building block (Fig. 5). These tetramers are linked via additional close S···N contacts (3.249(3) Å, 156.99(7)°), although the slightly smaller angle suggests this interaction is compromised in order to accommodate other packing forces. Notably the C-Br···N interactions present in both **1α** and **1β** are entirely absent in **1γ**. Instead one molecule forms a pair of F···S contacts (F15···S21 and F15···S22 at 3.238(2) and 3.152(2) Å) and a close Br···S contact (Br14···S12 at 3.531(1) Å, C-Br···S angle of 111.3(1)°) to a neighboring dimer (Fig. 5).

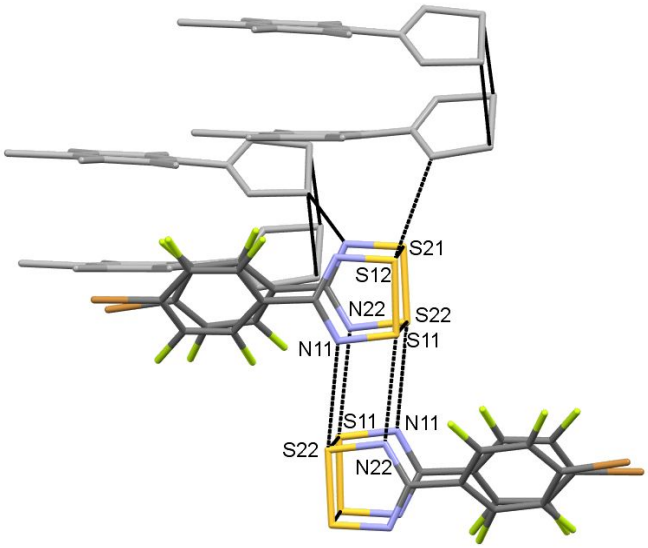

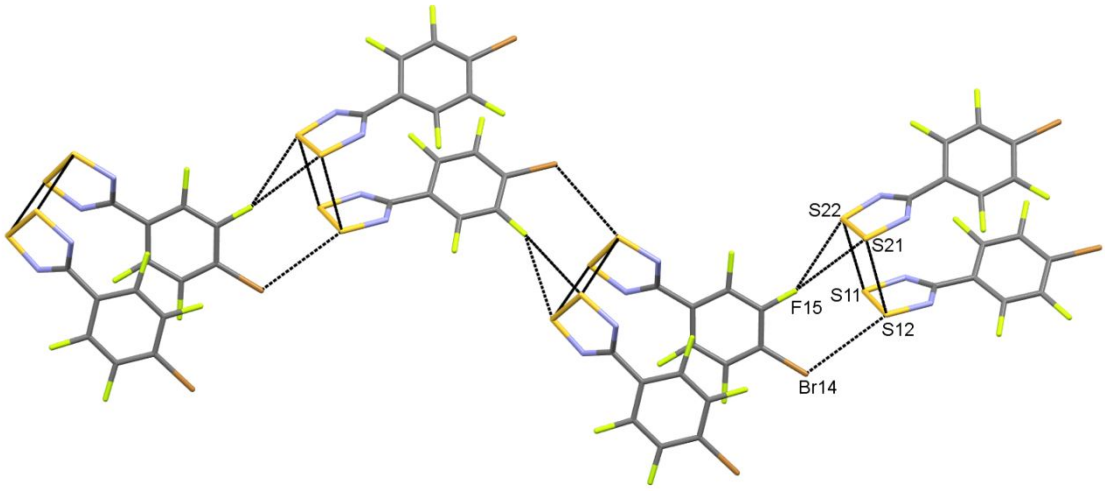

Figure 5: (top) The centrosymmetric 'dimer of dimers' motif of **1γ** with additional S···N contacts to neighboring dimers (gray) highlighted; (bottom) supramolecular chain motif in **1γ** linked through pairs of S···F and S···Br contacts.

Crystal structure of 2: The structure of **2** is isomorphous with **1α**. Given the isomorphous nature of **1α** and **2**, several sublimations of **2** were attempted with cold finger temperatures of −10 °C, −2 °C, and +6 °C (cold tap water) and oil bath temperatures of 70 °C. We expected that sub-zero cold finger temperatures (conditions which favored formation of **1β** or **1γ**) would favor partially or fully dimerized structures isomorphous to **1β** or **1γ**, but only a single phase has been isolated to date across a variety of sublimation conditions. Notably in both **1β** and **1γ** the structure-directing C-Br···N interaction is compromised to form other contacts. The lack of polymorphism in *p*-IC_6F_4CNSSN may be due to the enhanced strength of the C-I···N σ-hole interaction,[8] stabilizing the α-phase relative to other possible phases. Within **2** the torsion angle between DTDA and perfluoroaryl rings is 56.74° (*cf*. 51.77° for **1α**). The chain-forming C-I···N interaction has $d_{I\cdots N}$ = 3.121(7) Å and C-I···N angle of 164.3(2)° (Fig. 2), in good agreement with other C-I···N contacts (3.01(22) Å, 168(17)° SUP-3). The analogous S···N interaction to that in **1α** has an S···N distance of 3.254(7) and S- S···N angle of 158.1(2)° which is a little longer and exhibits a slightly more

acute angle than observed in **1α** (S···N at 3.17(1) Å, S-S···N at 160.2°), consistent with the slightly stronger structure-directing nature of this C-I···N interaction. Variable temperature PXRD (SUP-4) confirmed phase purity and the absence of other structural phases.

Structural Analysis: In order to probe polymorphism in **1** (and its absence in **2**) we undertook a series of computational studies. We implemented a combination of the dispersion-corrected unrestricted M06-2X-D3 functional for all calculations and a triple-zeta quality basis set (LACV3P*) which have been shown to provide good estimates of the strength of intermolecular forces such as halogen-bonding.[54] while the similar M06-D3 functional has provided reasonable geometries and enthalpies of dimerization in DTDA and DSDA radicals.[55]

Single point calculations on each of the crystallographically independent molecules in **1α**, **1β** and **1γ** were determined. These revealed that all the molecules of **1** are, within 2 kJ mol^{-1}, energetically equivalent (see ESI). This is consistent with the reported energy dependence for 2′,6′-difluoroaryl DTDA radicals which reveal a shallow potential well with a minimum torsion angle between rings near 50° with a range of twist angles from 20 – 90° falling within 5 kJ mol^{-1}.[56] In order to evaluate the strength of intermolecular forces in the different polymorphs of **1**, all nearest neighbor contacts with one or more intermolecular contacts less than the sum of the van der Waals radii were considered. Van der Waals forces reflect interactions which are short range in nature exhibiting a $1/r^6$ dependence[57] but contacts beyond the sum of the van der Waals radii can be significant and are particularly relevant for electrostatic contributions to bonding where a $1/r$ dependence is expected.[57] We therefore implemented the UNI force field model[58,59] within Mercury to check for additional significant contacts (> 5 kJ mol^{-1}) beyond the sum of the van der Waals radii. Taking **1α** as an example (with $Z' = 1$), a total of 10 nearest neighbor contacts representing 5 distinct intermolecular interactions less than the sum of the van der Waals radii

were identified and a further three interactions beyond the sum of the van der Waals radii with energies greater than 5 kJ mol^{-1} based on the UNI force field were additionally computed (Fig. 6). A corresponding analysis was undertaken for **1β**, **1γ** and **2** (see ESI).

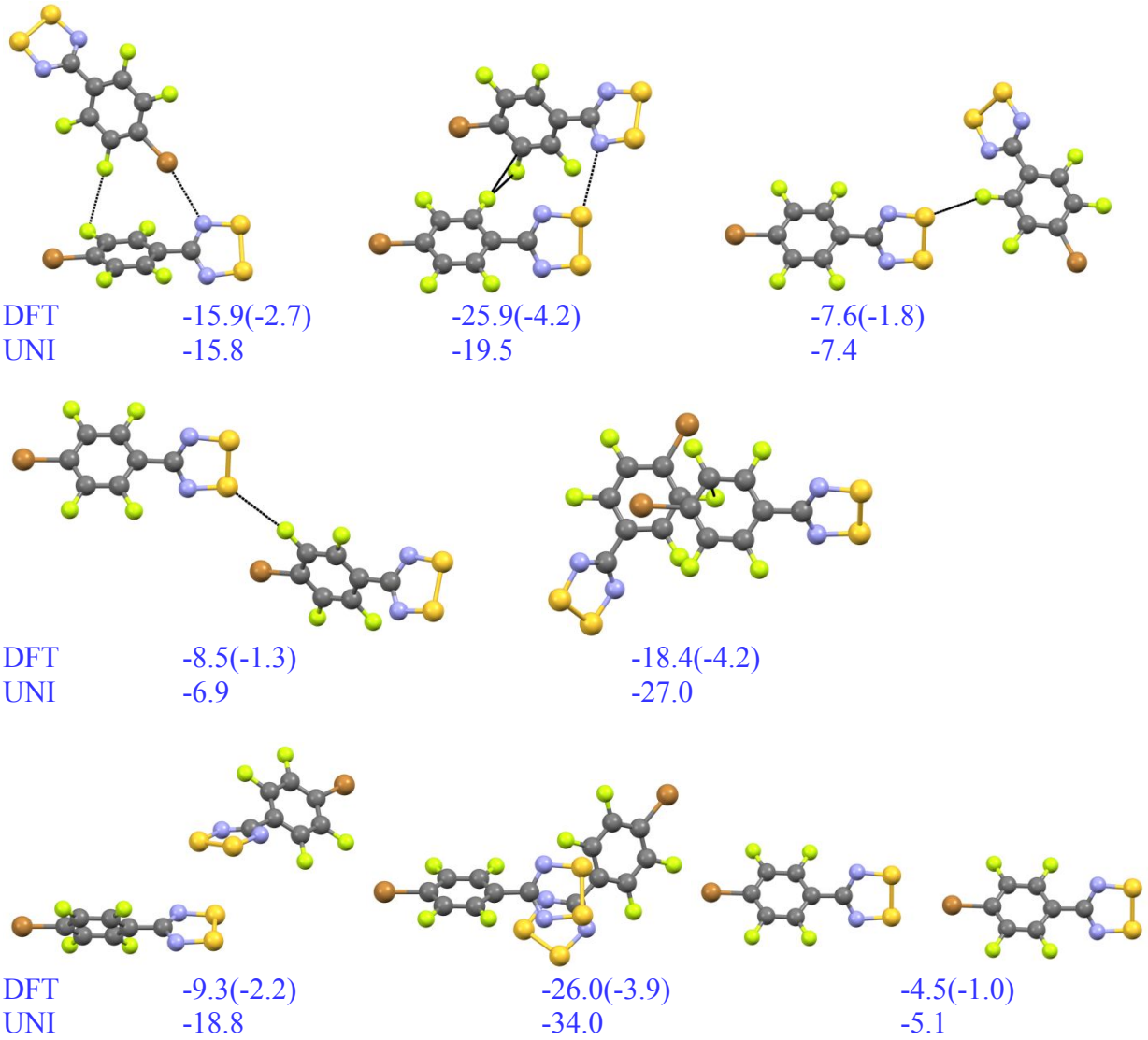

Figure 6: Intermolecular contacts in **1α** with contacts less than the sum of the van der Waals radii marked as dotted lines. The computed energies from DFT (UMO6-2X-D3/LACV3P*) and force field calculations (UNI) are presented below in kJ mol^{-1}. For the DFT calculations the contribution from dispersion is given in parentheses.

To evaluate the accuracy of the UNI force field to compute intermolecular potentials in DTDA radicals, 1SCF calculations (UMO6-2X-D3/LACV3P*) were computed as unrestricted triplets based on the crystallographic geometry of each radical pair. While the presence of magnetic exchange between nearest neighbors may mean that the triplet configuration may not be the ground state, the energy difference between open shell singlet (broken symmetry singlet) and triplet configurations is small when compared to the strength of these intermolecular interactions (typically less than 100 cm^{-1} and 1 kJ mol^{-1} = 84 cm^{-1})[60,61] and the triplet configurations typically converge more smoothly. The exception is the pancake bonding interactions observed in π*–π* dimers which were computed as unrestricted singlet configurations.[55] The energy of each interaction was determined by $E = E_{dimer} - (E_{rad1} + E_{rad2})$ where E_{dimer} is the open shell triplet and E_{rad1} and E_{rad2} are the energies of the two monomers. For cases with $Z' = 1$ (**1α** and **2**) then $E_{rad1} = E_{rad2}$ but for **1β** ($Z' = 3$) and **1γ** ($Z' = 2$) this was not generally the case.

While there is a clear positive correlation ($R^2 = 0.67$ based on 50 interactions considered in the three polymorphs of **1** and **2**, see ESI) between the intermolecular potentials computed through the UNI force-field and the DFT analysis, divergence between these values was not uncommon. In addition, several of the contacts which fall beyond the sum of the van der Waals radii are energetically significant based on both DFT and force-field approaches. This is particularly apparent for the π–π close contacts between DTDA rings in **1α** (Fig. 6 UNI-18.8 and UNI-34.0). The latter is perhaps unsurprising since the default parameters for determining van der Waals contacts are based on spherical van der Waals radii whereas analysis of crystal data has shown that elliptical radii are more appropriate, especially for heavier main group elements such as sulfur, bromine and iodine.[62] For these heavier elements contacts close to the molecular plane (minor radii) are typically shorter than those perpendicular (major van der Waals radii). In these two

radical pairs cited here (UNI-18.8 and UNI-34.0), the closest S…S contacts are 3.675 and 3.865 Å which both fall formally beyond the sum of the spherical van der Waals radii of sulfur (3.48 Å) but well within the sum of the major van der Waals radii for sulfur (4.06 Å). In this context consideration of close contacts might better be considered using ca. 1.16 times the spherical van der Waals radii for these heavier heteroatoms.

We also examined the stronger intermolecular interactions where structure-directing C-X…N and SN interactions appeared potentially significant. Here deviation between the UNI force field and DFT calculations were often disparate with DFT providing much larger interaction energies than the UNI force field model in the majority of cases (Table 2). The UNI force field approach is based on an atom-atom approach using an "exp-6" potential energy to optimize intermolecular interactions based on the distance between atoms.[58,59] This approach neglects electrostatic interactions (which may be significant in systems with strongly polar bonds which exhibit large partial positive and negative charges), covalent/charge-transfer interactions and dipole-dipole interactions. For strong halogen bonds there is a significant contribution from charge-transfer interactions and we implemented a natural bond order (NBO) analysis[63] to provide insight into individual contributions to the total interaction energy. A second order perturbation analysis of the Natural Bond Order calculations to not only probe the total strength of charge transfer interactions between molecules, but also to extract information on the relative contributions of C-X…N (X = Br, I) and SN interactions to the total interaction energy. The sum of the UNI plus charge-transfer interactions gave a much better correlation. Across the 50 interactions studies the R^2 value between DFT and UNI approaches was 0.67 but the selected 10 contacts highlighted in Table 2, where C-X….N and S…N contacts play an important role, exhibit an R^2 value of just 0.21 with a gradient of 0.53 suggesting (a) the UNI force field is relatively poor at analyzing these interactions and (b),

on average, under-estimates these interactions. significantly. A comparison of UNI+NBO-based CT interactions with DFT while still imperfect offered a much improved correlation ($R^2 = 0.56$) and a gradient of 0.88 suggesting the contribution from charge-transfer to these interactions is significant and provides much more reasonable estimates of the interaction energy.

Table 2: Energies of intermolecular interactions corresponding to C-X…N and S-S…N interactions in the structures of **1** and **2**. The interaction is denoted by the UNI code (reflecting the energy of the interaction based on the UNI force field potential) and reflect contacts depicted in Figure 6 (**1α**) and Figures S9 – S11(ESI). The total energy of the interaction based on the unrestricted MO6-2X-D3/LACV3P* calculations is presented, alongside the total contribution to the charge-transfer (CT) interaction derived from an NBO analysis. The final two columns represent the dominant contribution to this CT energy and its energy. All energies quoted in kJ/mol.

Compound	Interaction	DFT	NBO CT energy	Dominant contribution	Energy
1α	UNI -15.8	-15.9	-7.1	N(lp) to Br-C(σ*)	-3.5
	UNI-19.5	-25.9	-6.1	N(lp) to S-S (σ*) [SN-III]	-2.6
1β	UNI-10.4	-16.0	-6.7	N(lp) to Br-C(σ*)	-2.0
	UNI-10.6	-15.5	-4.9	N(lp) to Br-C(σ*)	-1.2
	UNI-12.7	-33.8	-13.2	N(lp) to S-N (σ*) [SN-I]	-4.9
	UNI-13.4	-27.4	-8.5	N(lp) to S-S (σ*) [SN-II]	-4.4
1γ	UNI-29.4	-33.8	-6.7	N(lp) to S-S (σ*) [SN-III]	-1.9
	UNI-12.0	-29.8	-14.3	N(lp) to S-S (σ*) [SN-II]	-5.7
2	UNI-21.3	-26.5	-11.4	N(lp) to I-C(σ*)	-7.2
	UNI-21.4	-25.1	-5.5	N(lp) to S-S (σ*) [SN-III]	-2.1

These NBO analyses also indicate that there is a significant σ-hole type interaction associated with the S…N contacts in addition to an electrostatic contribution. The breakdown of the total intermolecular charge-transfer energy into individual components allows the major contribution to each interaction to be determined (Table 2) and permits a comparison of the relative strengths of intermolecular S…N interactions (Fig. 1) with halogen bonds (Table 2). These reveal the charge-transfer contributions to these intermolecular interactions are C-I…N > SN-I > SN-II > C-Br…N > SN-III. The charge-transfer contribution to SN-II is approximately twice that observed

in SN-III due to the presence of two N lone pair to S-S σ* charge-transfer interactions in SN-II vs one similar interaction in SN-III. Overall, these observations reflect the strongly structure-directing nature of the C-I…N interaction in **2** while the more comparable energies of C-Br…N and S…N interactions are consistent with the prevalence for polymorphism in **1**. The computed dimerization energies for dimers in **1β** and **1γ** were computed as open shell singlets and found to be -21.6 and -11.7 kJ mol^{-1}. These interactions are weaker than those typically observed in solution (~-35 kJ mol^{-1})[31-33] but comparable with those estimated from SQUID or EPR data in the solid state (singlet-triplet energy of 7 – 18 kJ mol^{-1}).[16,24,37]

The behavior of **1β** is unusual in that its structure comprises a mixture of both monomeric and dimeric DTDA radicals, intermediate in nature between monomeric **1α** and dimeric **1γ**. Other examples where a mixture of monomers and dimers are observed include 2',6'-$F_2C_6H_3CNSSN$,[56,64] 2-ClC_6H_4CNSSN[37] , the sterically demanding 2',4',6'-$(F_3C)_3C_6H_2CNSSN$ derivative[65] and the 2,2'-biphenyl-4,4-bis(dithiadiazolyl radical).[66] In addition a number of radicals have been shown to undergo dynamic behavior in the solid state revealing progressive breakdown of the dimerization process. These include *p*-$EtOC_6F_4CNSSN$,[18] 2-Cl-5-X-C_6H_3CNSSN (X = Cl, I),[16] a biphenyl derivative,[67] a metallo-complex of a DTDA radical[68] and a recent benzimidazole derivative which exhibits an abrupt phase transition with thermal hysteresis.[15] The thermally-induced dynamic behavior is reminiscent of behavior observed in many π-stacked dithiazolyl radicals.[69-76]

DFT and Magnetic Studies: The magnetism of **1α** has been reported previously but with a total magnetic susceptibility reflecting just ca. 70% of the paramagnetism expected for an S = ½ paramagnet.[35] PXRD studies reveal that monomeric **1α** crystallizes concomitantly with **1β** under a range of conditions employed **(SUP-4)**. Since **1β** comprises a mixture of π*–π* dimers (which

are essentially diamagnetic) and monomers the original 70% S = ½ paramagnetism corresponds to ca 55% **1α** and 45%**1β**. The presence of **1β** therefore rationalizes the anomalously low susceptibility previously reported for **1α**. Unfortunately, since **1β** forms as a concomitant mix with **1α** we have been unable to perform susceptibility studies on either pure **1α** or pure **1β**. Nevertheless to gain some insight into the potential magnetism of **1β** close contacts between radical monomers were computed at the UB3LYP/6-311G* level of theory with a TZVP basis set used for Br atoms. The UB3LYP/6-311G* is known to reproduce well the sign and magnitude of the exchange couplings (J) in other DTDA radicals such as *p*-NCC_6F_4CNSSN and *p*-$O_2NC_6F_4CNSSN$.[60,61,77] The magnetic exchange interaction between two neighboring spins is defined by the spin Hamiltonian $H = -2JS_1 \cdot S_2$, where *J* is calculated from the energy, E, and expectation value, $<S^2>$, of the triplet (T) and broken symmetry singlet (BSS) using the approach of Yamaguchi:[78]

$$J = \frac{-(E_T - E_{BSS})}{<S^2>_T - <S^2>_{BSS}} \qquad \text{Eqn. 3}$$

For **1β** the network of close contacts between monomers generate a spin-ladder motif comprising three crystallographically distinct close contacts. The rail exchange ($J_{||}$) is less than the accuracy of the computations (0.1 cm^{-1}) and can be considered negligible. The remaining two exchange couplings comprise a ferromagnetic interaction $J_{\perp a}$ (+3.7 cm^{-1}) which is an order of magnitude greater than $J_{\perp b}$ (-0.2 cm^{-1}) (Fig. 7). The system is expected to behave as a very weakly ferromagnetically coupled dimer.

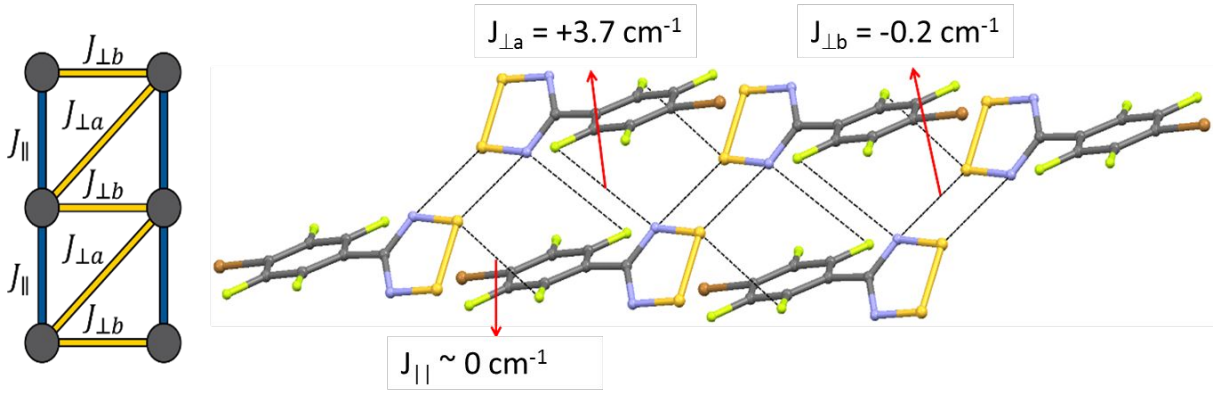

Figure 7: The spin ladder topology within the channels of **1β**

The structures of **1γ** is dimeric and such π*–π* dimers are well established to have singlet ground state configurations below ca. 250 K with the onset of weak paramagnetism arising from the presence of a thermally excited spin triplet on approaching room temperature.[16,24,30,37] In this context variable temperature magnetic studies were not undertaken on **1γ**.

The structure of **2** comprises purely monomers with several close contacts between heterocycles and is isomorphous with previously reported **1α**. However, since **2** appears devoid of polymorphs it appears as an excellent candidate to probe the magnetism of this structural topology. A polycrystalline sample of **2** (31 mg) was measured on a dc SQUID magnetometer in magnetic fields between 100 and 50000 Oe and temperatures from 1.8 – 300 K. Data were corrected for diamagnetism of the sample and the sample holder. In the high temperature regime (T > 50 K) the sample follows Curie-Weiss behavior (C = 0.376(2) emu·K·mol^{-1} and θ = -38.3(8) K, SUP-5). The Curie constant, C, is close to that expected for a simple S = ½ paramagnet with g = 2.005 (C = 0.376 emu·K·mol^{-1}), while the negative Weiss constant is consistent with net antiferromagnetic

interactions between spins. The temperature dependence of χT shows a room temperature value of χT (0.340 emu·K·mol^{-1}) which decreases slowly down to *ca*. 70 K and then decreases more rapidly to ~ 0 emu·K·mol^{-1} as T approaches zero Kelvin, consistent with short-range antiferromagnetic interactions (Fig. 8). The temperature dependence of χ is more informative, showing the initial increase in χ expected for an S = ½ paramagnet (χ ∝ T^{-1}), followed by passing through a broad maximum in χ at 20 K diagnostic of short range (low dimensional) antiferromagnetic ordering (Fig. 8). At low temperature (< 3.8 K) there is a small increase in χ consistent with a small contribution from S = ½ lattice defects.

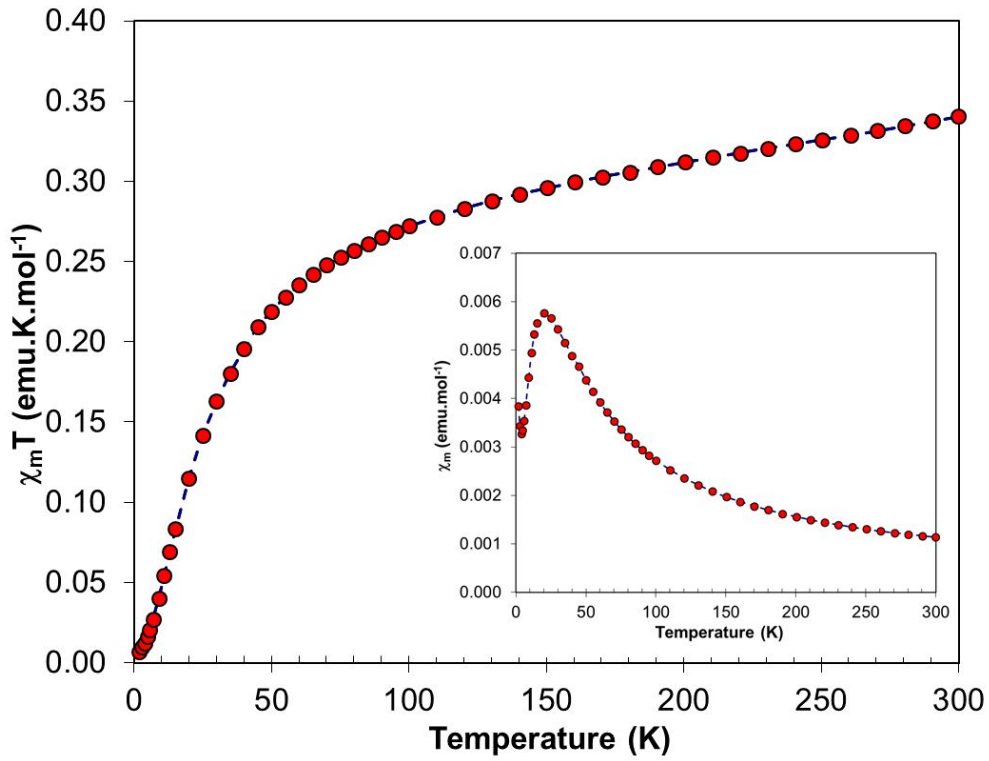

Figure 8: Temperature dependence of $\chi_m T$ with (inset) temperature dependence of χ_m for **2** [The dashed line is merely a guide to the eye].

In order to identify an appropriate magnetic model, single point DFT calculations on **2** were made using the B3LYP method and 6-31G* or 6-311G* basis sets for the light atoms and an LAV3P+ effective core potential for iodine. This approach showed good convergence between basis sets for both J_1 and J_3 which were antiferromagnetic. While more variation in the value of J_2 was observed, both levels of theory predicted J_2 to be ferromagnetic, consistent with the signs and magnitudes of J_1, J_2 and J_3 previously computed for isomorphous **1α**.[60,61] An analysis of the exchange coupling pathways revealed a complex two-dimensional exchange pathway (Fig. 9). The dominant exchange pathway, J_1, is a factor of 2 – 3 larger than J_2 and J_3 at the B3LYP/6-31G*/LAV3P* level of theory. Initial attempts to model the system as a simple dimer model using the Bleaney-Bowers expression[79] required large mean field terms θ, comparable to $|J_{intra}/k|$, to provide a satisfactory fit to the data. This is unsurprising as such mean field approximations tend to only hold well when the interdimer interactions are a magnitude smaller than J_{intra}. We also investigated a one-dimensional alternating chain model[79] but again a large mean field constant was required,

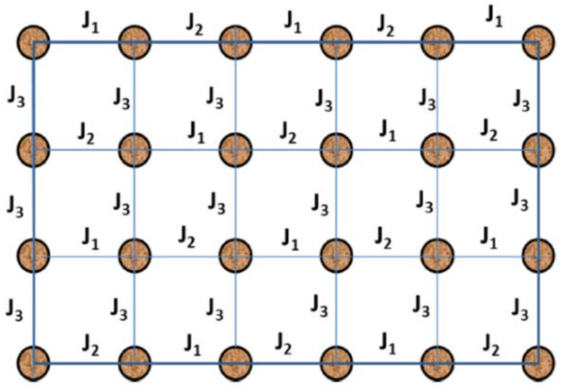

1α

Exchange	Basis Set: 6-31G**	6-311G**
J_1 (cm^{-1})	-10	-8
J_2 (cm^{-1})	+9	+8
J_3 (cm^{-1})	-8	-8

2

Exchange	Basis Set: 6-31G*+LAV3P*	6-311G*+LAV3P*
J_1 (cm^{-1})	-24	-22
J_2 (cm^{-1})	+8	+2
J_3 (cm^{-1})	-9	-9

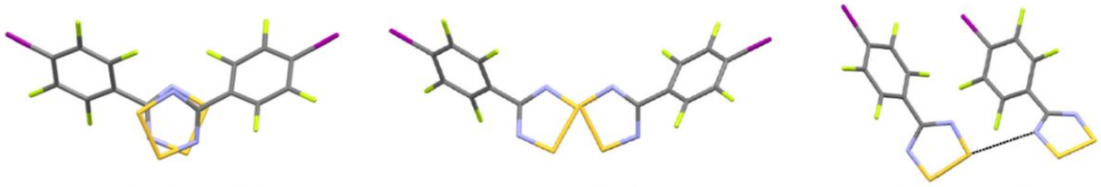

1α	S…S 3.865	S…S 3.675	S…N 3.175
2	S…S 3.927	S…S 3.741	S…N 3.254

Figure 9: (top left) exchange pathways between radicals in both **1α** and **2**; (top right) computed exchange couplings for **1α** and **2**; (bottom) nature of the close contacts associated with J_1, J_2 and J_3 (from left to right respectively).

reflecting a more complex magnetic system (see SUP-5). Since the magnitudes of the computed exchange couplings (Fig 9) are similar for all three communication pathways it is not possible to approximate this system to a simpler model. In this context we resort to the mean field model where the macroscopic Weiss constant is related to the individual exchange constants according to:[79]

$$\theta = \frac{-2\sum J_i S(S+1)}{3k} \qquad \text{Eqn. 4}$$

which comprises a sum over all nearest neighbor exchange couplings. In this case this comprises J_1, J_2 and two symmetry equivalent J_3 interactions (Fig. 9) and at the B3LYP/6-31G* level of theory with LACVP+ basis set for iodine, θ = -25 K, comparable with the experimental Weiss constant (θ = -38 K).

DISCUSSION

The computed C-I…N σ-hole interaction (-26.5 kJ mol^{-1}) for **2** is in good agreement with previous studies have indicated that the C-I···N interaction energy in 4,4'-dipyridyl/1,4-di-iodotetrafluorobenzene, a prototypical *sp*^{2} nitrogen σ-hole interaction, is *ca*. 24 kJ/mol.[8,80] The corresponding C-Br…N interactions in **1** average around -15.8 kJ mol^{-1} , again corresponding well to the weaker nature of this interaction in relation to the C-I…N halogen bond. The computed π*–π* dimerization energies in **1β** and **1γ** (-21.6 and -11.7 kJ mol^{-1}) are also in good agreement with experimental estimates of dimerization based on solid state magnetic measurements and EPR data (singlet-triplet energy gap of 7 – 18 kJ mol^{-1}).[16,24,37] The nature of the intermolecular S…N contacts between DTDA radicals has been described as having an important electrostatic

contribution.[48] The current studies reveal that there is also an significant contribution arising from charge transfer which can be considered as a sigma-hole interaction associated with nitrogen lone pair donation into S-S σ* (SN-II, SN-III) or S-N σ* orbitals (SN-I). These interactions are energetically comparable with the more established halogen bonds. In this context a search of the CSD for C-Br…N, C-I…N and S-S…N interactions proved instructive. The strongest C-I…N interaction exhibits a strong angular and distance dependence of the interaction with a maximum in the distribution of C-I…N distances at 2.8 Å (SUP-3). Conversely while both C-Br…N and S-S…N exhibit a strong angular dependence (SUP-1 and SUP-2) there is no clear maximum in the intermolecular contact, indicative of a weaker interaction. Competition between these two comparable sets of intermolecular forces is likely the origin of the polymorphism in **1**.

CONCLUSIONS

A total of three polymorphs of radical **1** were isolated, comprising a pair of concomitant polymorphs (**1α** and **1β**) plus a third polymorph (**1γ**) which can be isolated at elevated temperatures. A study of the different polymorphs of **1** was undertaken using a combination of the UNI force-field model and DFT calculations of the intermolecular interactions. These reveal that caution should be applied when reviewing intermolecular contacts in terms of van der Waals radii. Some close contacts between molecules do not contribute significantly to the intermolecular forces whereas some contacts beyond the sum of the van der waals radii are significant. In part this arises from the anisotropy in the van der Waals radius for heavier p-block elements. While there was a general qualitative agreement between the two methods, quantitative analysis of these interactions revealed significant deviations particularly for robust structure-directing interactions in which covalency/charge transfer is neglected in the UNI model. DFT coupled with a second order NBO

analysis reveal the presence of robust sigma-hole interactions (i.e. lp → σ*) in both C-Br…N and S…N interactions. For the iodo derivative **2**, the C-I…N interaction is computed to be more robust than the corresponding C-Br…N interaction and a single phase of **2** was identified (isomorphous with **1α**) under a range of sublimation conditions, suggesting this packing motif optimizes this dominant intermolecular interaction. In **1** the C-Br…N and S…N interactions are comparable and there is competition between alternative packing motifs.

ASSOCIATED CONTENT

The following files are available free of charge:

Supplementary data in pdf file format

Crystallographic data in cif file format

AUTHOR INFORMATION

Corresponding Author

* J. M. Rawson, Dept of Chemistry & Biochemistry, The University of Windsor, 401 Sunset Avenue, Windsor, ON N9B 3P4 CANADA. E-mail: jmrawson@uwindsor.ca

Present Addresses

† School of Chemistry, The University of Leeds, Leeds, UK, LS2 9JT.

Author Contributions

The manuscript was written through contributions of all authors. All authors have given approval to the final version of the manuscript.

Funding Sources

We would like to thank the NSERC DG program for financial support (J.M.R.) and C.F.I./O.R.F. for an infrastructure grant. M.A.N. would like to thank the NSERC for a CGS-M scholarship. J.C. acknowledges support from grant PGC-2018-099024-B100. Additional support from Diputación General de Aragon (DGA-M4) is also acknowledged. J.C and A.A. would like to acknowledge the use of Servicio General de Apoyo a la Investigación-SAI, Universidad de Zaragoza.

References

1 Nangia, A. K.; Desiraju, G. R., Crystal Engineering: An Outlook for the Future. *Angew. Chem. Int. Ed.* **2019**, *58* (13), 4100-4107.

2 G. R. Desiraju, *The Weak Hydrogen Bond: In Structural Chemistry and Biology*, Oxford University Press (2001).

3 G. Gilli; P. Gilli, "*The Nature of the Hydrogen Bond: Outline of a Comprehensive Hydrogen Bond Theory*", Oxford University Press (2009).

4 Dunitz, J. D.; Gavezzotti, A., Supramolecular Synthons: Validation and Ranking of Intermolecular Interaction Energies. *Cryst. Growth Des.* **2012**, *12* (12), 5873-5877.

5 Cruz-Cabeza, A. J.; Reutzel-Edens, S. M.; Bernstein, J., Facts and fictions about polymorphism. *Chem. Soc. Rev.* **2015**, *44* (23), 8619-8635.

6 Cordes, A. W.; Haddon, R. C.; Oakley, R. T., Molecular conductors from neutral heterocyclic π-radicals. *Adv. Mater.* **1994**, *6* (10), 798-802.

7 Rawson, J. M.; Constantinides, C. *Thiazyl-Based Magnets*, Chapter 2 (pp. 95-124) in "Spin in Organics, volume IV" (J.S. Miller, Ed.), World Scientific, 2018.

8 Cavallo, G.; Metrangolo, P.; Milani, R.; Pilati, T.; Priimagi, A.; Resnati, G.; Terraneo, G., The Halogen Bond. *Chem. Rev.* **2016**, *116* (4), 2478-2601.

9 Nascimento, M. A.; Rawson, J. M., *1,2,3,5-Dithiadiazolyl Radicals* in "the Encyclopedia of Inorganic and Bioinorganic Chemistry", Wiley, 2019.

10 Rawson, J. M.; Alberola, A.; Whalley, A., Thiazyl radicals: old materials for new molecular devices. *J. Mater. Chem.* **2006**, *16* (26), 2560-2575.

11 Preuss, K. E., Metal complexes of thiazyl radicals. *Dalton Trans.* **2007**, 2357-2369.

12 Preuss, K. E., Metal-radical coordination complexes of thiazyl and selenazyl ligands. *Coord. Chem. Rev.* **2015**, *289-290*, 49-61.

13 Banister, A. J.; May, I.; Rawson, J. M.; Smith, J. N. B., Dithiadiazolyls as heterocyclic chelators: a radical approach to coordination chemistry? *J. Organomet. Chem.* **1998**, *550* (1), 241-253.

14 Y. Mnyukh, *Fundamentals of Solid-State Phase Transitions, Ferromagnetism and Ferroelectricity*, First books, 2001.

15 Mills, M. B.; Wohlhauser, T.; Stein, B.; Verduyn, W. R.; Song, E.; Dechambenoit, P.; Rouzières, M.; Clérac, R.; Preuss, K. E., Magnetic Bistability in Crystalline Organic Radicals: The Interplay of H-bonding, Pancake Bonding, and Electrostatics in 4-(2′-Benzimidazolyl)-1,2,3,5-dithiadiazolyl. *J. Am. Chem. Soc.* **2018**, *140* (49), 16904-16908.

16 Constantinides, C. P.; Carter, E.; Eisler, D.; Beldjoudi, Y.; Murphy, D. M.; Rawson, J. M., Effects of Halo-Substitution on 2'-Chloro-5'-halo-phenyl-1,2,3,5-dithiadiazolyl Radicals: A Crystallographic, Magnetic, and Electron Paramagnetic Resonance Case Study. *Cryst. Growth Des.* **2017**, *17* (6), 3017-3029.

17 Beldjoudi, Y.; Arauzo, A.; Campo, J.; Gavey, E.L.; Pilkington, M; Nascimento, M. A.; Rawson, J. M. Structural, Magnetic, and Optical Studies of the Polymorphic 9'-Anthracenyl Dithiadiazolyl Radical. *J. Amer. Chem. Soc*., **2019**, *141* (17), 6875 – 6889.

18 Beldjoudi, Y.; Sun, R.; Arauzo, A.; Campo, J.; Less, R. J.; Rawson, J. M., Structural Variations in the Dithiadiazolyl Radicals *p*-ROC_6F_4CNSSN (R = Me, Et, ^{n}Pr, ^{n}Bu): A Case Study of Reversible and Irreversible Phase Transitions in *p*-$EtOC_6F_4CNSSN$. *Cryst. Growth Des.* **2018**, *18* (1), 179-188.

19 Haynes, D. A., Crystal engineering with dithiadiazolyl radicals. *CrystEngComm* **2011**, *13* (15), 4793-4805.

20 Haynes, D. A.; Rawson, J.M. Molecular Electrostatic Potential as a Predictor of Supramolecular Synthons in Non-Hydrogen-Bonded Systems: Application to Heavier *p*-Block Systems, *Eur. J. Inorg. Chem.*, **2018** (31), 3556 – 3564.

21 Cordes, A. W.; Haddon, R. C.; Hicks, R. G.; Oakley, R. T.; Palstra, T. T. M., Preparation and solid-state structures of (cyanophenyl)dithia- and (cyanophenyl)diselenadiazolyl radicals. *Inorg. Chem.* **1992**, *31* (10), 1802-1808.

22 Lau, H. F.; Ng, V. W. L.; Koh, L. L.; Tan, G. K.; Goh, L. Y.; Roemmele, T. L.; Seagrave, S. D.; Boeré, R. T., Cyclopentadienylchromium Complexes of 1,2,3,5-Dithiadiazolyls: η^2 π Complexes of Cyclic Sulfur–Nitrogen Compounds. *Angew. Chem. Int. Ed.* **2006**, *45* (27), 4498-4501.

23 Cordes, A. W.; Chamchoumis, C. M.; Hicks, R. G.; Oakley, R. T.; Young, K. M.; Haddon, R. C., Mono- and difunctional furan-based 1,2,3,5-dithiadiazolyl radicals; preparation and solid state structures of 2,5-[$(S_2N_2C)OC_4H_2(CN_2S_2)$] and 2,5-[$(S_2N_2C)OC_4H_2(CN)$]. *Can. J. Chem.* **1992**, *70* (3), 919-925.

24 Shuvaev, K. V.; Decken, A.; Grein, F.; Abedin, T. S. M.; Thompson, L. K.; Passmore, J., NC–$(CF_2)_4$–CNSSN containing 1,2,3,5-dithiadiazolyl radical dimer exhibiting triplet excited states at low temperature and thermal hysteresis on melting–solidification: structural, spectroscopic, and magnetic characterization. *Dalton Trans.* **2008**, 4029-4037.

25 Antorrena, G.; Brownridge, S.; Cameron, T. S.; Palacio, F.; Parsons, S.; Passmore, J.; Thompson, L. K.; Zarlaida, F., The neutral diradical 5,5'-bis(1,3,2,4-dithiadiazolyl), the first main group radical to exhibit a dramatic increase in paramagnetism on mechanical grinding. *Can. J. Chem.* **2002**, *80* (11), 1568-1583.

26 Banister, A. J.; Bricklebank, N.; Clegg, W.; Elsegood, M. R. J.; Gregory, C. I.; Lavender, I.; Rawson, J. M.; Tanner, B. K., The first solid state paramagnetic 1,2,3,5-dithiadiazolyl radical; X-ray crystal structure of [*p*-NCC_6F_4CNSSN]. *J. Chem. Soc., Chem. Commun.* **1995**, 679-680.

27 Banister, A. J.; Bricklebank, N.; Lavender, I.; Rawson, J. M.; Gregory, C. I.; Tanner, B. K.; Clegg, W.; Elsegood, M. R. J.; Palacio, F., Spontaneous Magnetization in a Sulfur–Nitrogen Radical at 36 K. *Angew. Chem. Int. Ed.* **1996**, *35* (21), 2533-2535.

28 Alberola, A.; Less, R. J.; Palacio, F.; Pask, C. M.; Rawson, J. M., Synthesis and Magnetic Properties of the Novel Dithiadiazolyl Radical, *p*-$NCC_6F_4C_6F_4CNSSN$. *Molecules* **2004**, *9* (9), 771-781.

29 Kertesz, M., Pancake Bonding: An Unusual Pi-Stacking Interaction. *Chem. Eur. J.* **2019**, *25* (2), 400-416.

30 Preuss, K. E., Pancake bonds: π-Stacked dimers of organic and light-atom radicals. *Polyhedron* **2014**, *79*, 1-15.

31 Fairhurst, S. A.; Johnson, K. M.; Sutcliffe, L. H.; Preston, K. F.; Banister, A. J.; Hauptman, Z. V.; Passmore, J., Electron spin resonance study of $CH_3CNSSN^{\bullet}$, $C_6H_5CNSSN^{\bullet}$, and $SNSSN^{\bullet+}$ free radicals. *J. Chem. Soc., Dalton Trans.* **1986**, 1465-1472.

32 Brooks, W. V. F.; Burford, N.; Passmore, J.; Schriver, M. J.; Sutcliffe, L. H., Paramagnetic liquids: the preparation and characterisation of the thermally stable radical $Bu^tCNSNS^{\bullet}$ and its quantitative photochemically symmetry allowed rearrangement to a second stable radical $Bu^tCNSSN^{\bullet}$. *J. Chem. Soc., Chem. Commun.* **1987**, 69-71.

33 Britten, J.; Hearns, N. G. R.; Preuss, K. E.; Richardson, J. F.; Bin-Salamon, S., Mn(II) and Cu(II) Complexes of a Dithiadiazolyl Radical Ligand: Monomer/Dimer Equilibria in Solution. *Inorg. Chem.* **2007**, *46* (10), 3934-3945.

34 Boeré, R. T.; Hill, N. D. D., High Z' structures of 1,2,3,5-dithiadiazolyls and of 1,2,3,5-diselenadiazolyls containing the first structurally characterized monomeric diselenadiazolyls. *CrystEngComm* **2017**, *19* (26), 3698-3707.

35 Antorrena, G.; Palacio, F.; Davies, J. E.; Hartley, M.; Rawson, J. M.; Smith, J. N. B.; Steiner, A., A novel paramagnetic dithiadiazolyl radical: Crystal structure and magnetic properties of *p*-$BrC_6F_4CNSSN^{\bullet}$. *Chem. Commun.* **1999**, 1393-1394.

36 Beldjoudi, Y.; Arauzo, A.; Palacio, F.; Pilkington, M.; Rawson, J. M., Studies on a "Disappearing Polymorph": Thermal and Magnetic Characterization of α-*p*-$NCC_6F_4CNSSN^{\bullet}$. *J. Am. Chem. Soc.* **2016**, *138* (51), 16779-16786.

37 Constantinides, C. P.; Eisler, D. J.; Alberola, A.; Carter, E.; Murphy, D. M.; Rawson, J. M., Weakening of the π*–π* dimerisation in 1,2,3,5-dithiadiazolyl radicals: structural, EPR, magnetic and computational studies of dichlorophenyl dithiadiazolyls, $Cl_2C_6H_3CNSSN$. *CrystEngComm* **2014**, *16* (31), 7298-7312.

38 Desiraju, G. R., *Crystal engineering: The Design of Organic Solids,* Materials Science Monographs vol. 54, Elsevier Press, 1989.

39 Desiraju, G. R., Designing organic crystals. *Prog. Solid State Chem.* **1987**, *17* (4), 295-353.

40 Birchall, J. M.; Haszeldine, R. N.; Jones, M. E., Polyfluoroarenes. Part XVII. Some reactions of pentafluorobenzonitrile. *J. Chem. Soc. C* **1971**, 1343-1348.

41 APEX3, Bruker AXS, Madison, WI, USA.

42 SAINT, Bruker AXS, Madison, WI, USA.

43 SADABS, Bruker AXS, Madison, WI, USA.

44 Sheldrick, G. M., *Acta Cryst.*, 2015, A**71**, 3.

45 Sheldrick, G. M., *Acta Cryst.,* 2015, C**71**, 3.

46 Boeré, R. T.; Oakley, R. T.; Reed, R. W., Preparation of N,N,N-tris(trimethylsilyl)amidines; a convenient route to unsubstituted amidines. *J. Organomet. Chem.* **1987**, *331* (2), 161-167.

47 Robinson, S. W.; Haynes, D. A.; Rawson, J. M., Co-crystal formation with 1,2,3,5-dithiadiazolyl radicals. *CrystEngComm* **2013**, *15* (47), 10205-10211.

48 Bond, A. D.; Haynes, D. A.; Pask, C. M.; Rawson, J. M., Concomitant polymorphs: structural studies on the trimorphic dithiadiazolyl radical, ClCNSSN. *J. Chem. Soc., Dalton Trans.* **2002**, 2522-2531.

49 Clarke, C. S.; Pascu, S. I.; Rawson, J. M., Further studies on the polymorphic dithiadiazolyl radical, ClCNSSN. *CrystEngComm* **2004**, *6* (17), 79-82.

50 Knapp, C.; Lork, E.; Gupta, K.; Mews, R. Structure Investigations on 4-Halo-1,2,3,5-dithiadiazolyl Radicals XCNSSN$^{\bullet}$ (X = F, Cl, Br): The Shortest Intradimer S···S Distance in Dithiadiazolyl Dimers, *Z.Anorg.Allg.Chem.*, **2005**, *631*, 1640 - 1644.

51 Bernstein, J. *Polymorphism in Molecular Crystals*, Oxford University Press (2007).

52 Bernstein, J.; Davey, R. J.; Henck, J.-O., Concomitant Polymorphs. *Angew. Chem. Int. Ed.* **1999**, *38* (23), 3440-3461.

53 Alberola, A.; Less, R. J.; Pask, C. M.; Rawson, J. M.; Palacio, F.; Oliete, P.; Paulsen, C.; Yamaguchi, A.; Farley, R. D.; Murphy, D. M., A Thiazyl-Based Organic Ferromagnet. *Angew. Chem. Int. Ed.* **2003**, *42* (39), 4782-4785.

54 Siiskonen, A.; Priimagi, A. Benchmarking DFT methods with small basis sets for the calculation of halogen-bond strengths, *J. Mol. Model.*, **2017**, *23*, 50.

55 Melen, R.L.; Less, R.J.; Pask, C.M.; Rawson, J.M.; Structural Studies of Perfluoroaryldiselenadiazolyl Radicals: Insights into Dithiadiazolyl Chemistry, *Inorg. Chem.*, **2016**, *55*, 11747−11759.

56 Clarke, C. S.; Haynes, D. A.; Smith, J. N. B.; Batsanov, A. S.; Howard, J. A. K.; Pascu, S. I.; Rawson, J. M., The effect of fluorinated aryl substituents on the crystal structures of 1,2,3,5-dithiadiazolyl radicals. *CrystEngComm* **2010**, *12* (1), 172-185.

57 Atkins, P.; de Paula, J.; Keeler, J. Atkins' Physical Chemistry, 11th Ed. Oxford University Press, **2018**.

58 Gavezzotti, A.; Filippini, G. Geometry of the Intermolecular X-H.cntdot..cntdot..cntdot.Y (X, Y = N, O) Hydrogen Bond and the Calibration of Empirical Hydrogen-Bond Potentials, *J. Phys. Chem.* **1994**, 98(18), 4831-4837.

59 Gavezotti, A. Are Crystal Structures Predictable?, *Acc. Chem. Res.* **1994**, 27 (10), 309-314.

60 Rawson, J. M.; Luzon, J.; Palacio, F., Magnetic exchange interactions in perfluorophenyl dithiadiazolyl radicals. *Coord. Chem. Rev.* **2005**, *249* (23), 2631-2641.

61 Luzón, J.; Campo, J.; Palacio, F.; McIntyre, G. J.; Rawson, J. M., Ab initio study of the magnetic behavior of four dithiadiazolyl radical compounds. *Polyhedron* **2005**, *24* (16), 2579-2583.

62 Nyburg, S. C.; Faerman, C. H. A revision of van der Waals atomic radii for molecular crystals: N, O, F, S, Cl, Se, Br and I bonded to carbon, *Acta Cryst.* **1985**, *B41*, 274-279.

63 Weinhold, F.; Landis, C.R., Natural Bond Orbitals and extensions of localized bonding concepts, *Chem. Ed.*, **2001**, *2*, 91 – 104.

64 Fatila, E.M.; Jennings, M. C.; Goodreid, J.; Preuss, K.E., A third polymorph of 4-(2,6-difluorophenyl)-1,2,3,5-dithiadiazolyl, *Acta Cryst.* **2010**, *C66*, o260-o264.

65 Alberola, A.; Clarke, C.S.; Haynes, D.A.; Pascu, S.I.; Rawson J.M. Crystal structures and magnetic properties of a sterically encumbered dithiadiazolyl radical, 2,4,6-$(F_3C)_3C_6H_2CNSSN$, *Chem. Commun.*, **2005**, 4726 – 4728.

66 Barclay, T.M.; Cordes, A.W.; George, N.A.; Haddon, R.C.; Itkis, M. E.; Oakley, R.T. A bimodal dithiadiazolyl diradical: crystal structure and magnetic properties of the 2,2'-dimethylbiphenylene bridged derivative, *Chem. Commun.*, **1999**, 2269- 2270.

67 Suizu, R.; Iwasaki, A.; Schuko, Y.; Awaha, K. Spatially inhomogeneous, stepwise phase transitions in a thiazyl diradical: a structural mismatch induced by lattice transformation, *J. Mater. Chem. C.*, **2015**, 3, 7968 - 7977.

68 Fatila, E.M.; Mayo, R.A.; Rouzieres, M.; Jennings, M.C.; Dechambenoit, P.; Soldatov, D.V.; Mathoniere, C.; Clerac, R.; Coulon, C.; Preuss, K.E. Radical–Radical Recognition: Switchable Magnetic Properties and Re-entrant Behavior, *Chem. Mater*. **2015**, 27, 4023-4032.

69 Brusso, J.L.; Clements, O.P.; Haddon, R.C.; Itkis, M.E.; Leitch, A.A.; Oakley, R.T.; Reed, R.W.; Richardson, J.F., Bistability and the Phase Transition in 1,3,2-Dithiazolo[4,5-b]pyrazin-2-yl, *J. Am. Chem. Soc*. **2004**, 126, 14692-14693.

70 Brusso, J.L.; Clements, O.P.; Haddon, R.C.; Itkis, M.E.; Leitch, A.A.; Oakley, R.T.; Reed, R.W.; Richardson, J.F., Bistability and the Phase Transition in 1,3,2-Dithiazolo[4,5-b]pyrazin-2-yl, *J. Am. Chem. Soc*. **2004**, 126, 8256-8265.

71 Fujita, W.; Awaga, K. Room-Temperature Magnetic Bistability in Organic Radical Crystals, *Science*, **1999**, 286, 261 – 262.

72 Alberola, A.; Collis, R. J.; Humphrey, S.M.; Less, R.J.; Rawson, J.M. Spin Transitions in a Dithiazolyl Radical: Preparation, Crystal Structures, and Magnetic Properties of 3-Cyanobenzo-1,3,2-dithiazolyl, $C_7H_3S_2N_2$, *Inorg. Chem.*, **2006**, 45, 1903-1905.

73 McManus, G.D.; Rawson, J.M.; Feeder, N.; van Duijn, J.; McInnes, E.J.L.; Novoa, J.J.; Burriel, R.; Palacio, F.; Oliete, P. Synthesis, crystal structures, electronic structure and magnetic behaviour of the trithiatriazapentalenyl radical, $C_2S_3N_3$, *J. Mater. Chem.*, **2001**,11, 1992-2003.

74 Francese, T.; Mota, F.; Deumal, M.; Novoa, J.J.; Havenith, R.W.A.; Broer, R.; Ribas-Arino, J. Reorganization of Intermolecular Interactions in the Polymorphic Phase Transition of a Prototypical Dithiazolyl-Based Bistable Material, *Cryst. Growth Des.* **2019**, 19, 2329-2339.

75 Francese, T.; Ribas-Arino, J.; Novoa, J.J.; Havenith, R.W.A.; Broer, R.; Deumal, M., The magnetic fingerprint of dithiazolyl-based molecule magnets, *Phys. Chem. Chem. Phys.*, **2018**, 20, 20406-20416.

76 Vela, S.; Reardon, M.B.; Jakobsche, C.E.; Turnbull, M.M.; Ribas-Arino, J.; Novoa, J.J. Bistability in Organic Magnetic Materials: A Comparative Study of the Key Differences between Hysteretic and Non-hysteretic Spin Transitions in Dithiazolyl Radicals, *Chem.- Eur. J.*, **2017**, 23, 3479 – 2489.

77 Deumal, M.; Rawson, J. M.; Goeta, A. E.; Howard, J. A. K.; Copley, R. C. B.; Robb, M. A.; Novoa, J. J., Studying the Origin of the Antiferromagnetic to Spin-Canting Transition in the α-*p*-NCC_6F_4CNSSN Molecular Magnet. *Chem. Eur. J.* **2010**, *16* (9), 2741-2750.

78 Nagao, H.; Nishino, M.; Shigeta, Y.; Soda, T.; Kitagawa, Y.; Onishi, T.; Yoshioka, Y.; Yamaguchi, K., Theoretical studies on effective spin interactions, spin alignments and macroscopic spin tunneling in polynuclear manganese and related complexes and their mesoscopic clusters. *Coord. Chem. Rev.* **2000**, *198* (1), 265-295.

79 Carlin, R.L. *Magnetochemistry*, Springer-Verlag (1986). (replacing *z*J by ΣJ to take into account differing exchange couplings).

80 Walsh, R. B.; Padgett, C. W.; Metrangolo, P.; Resnati, G.; Hanks, T. W.; Pennington, W. T., Crystal Engineering through Halogen Bonding: Complexes of Nitrogen Heterocycles with Organic Iodides. *Cryst. Growth Des.* **2001**, *1* (2), 165-175.